



Optics Letters

Accurate quantitative phase imaging by the transport of intensity equation: a mixed-transfer-function approach

LINPENG LU,^{1,2} YAO FAN,^{1,2} JIASONG SUN,^{1,2} JIALING ZHANG,^{1,2} XUEJUAN WU,^{1,2} QIAN CHEN,^{2,3}  AND CHAO ZUO^{1,2,*} 

¹Smart Computational Imaging Laboratory (SCILab), School of Electronic and Optical Engineering, Nanjing University of Science and Technology, Nanjing, Jiangsu Province 210094, China

²Jiangsu Key Laboratory of Spectral Imaging & Intelligent Sense, Nanjing University of Science and Technology, Nanjing, Jiangsu Province 210094, China

³e-mail: chenqian@njjust.edu.cn

*Corresponding author: zuochao@njjust.edu.cn

Received 5 February 2021; revised 3 March 2021; accepted 4 March 2021; posted 5 March 2021 (Doc. ID 422095); published 29 March 2021

As a well-established deterministic phase retrieval approach, the transport of intensity equation (TIE) is able to recover the quantitative phase of a sample under coherent or partially coherent illumination with its through-focus intensity measurements. Nevertheless, the inherent paraxial approximation limits its validity to low-numerical-aperture imaging and slowly varying objects, precluding its application to high-resolution quantitative phase imaging (QPI). Alternatively, QPI can be achieved by phase deconvolution approaches based on the coherent contrast transfer function or partially coherent weak object transfer function (WOTF) without invoking paraxial approximation. But these methods are generally appropriate for “weakly scattering” samples in which the total phase delay induced by the object should be small. Consequently, high-resolution high-accuracy QPI of “nonweak” phase objects with fine details and large phase excursions remains a great challenge. In this Letter, we propose a mixed-transfer-function (MTF) approach to address the dilemma between measurement accuracy and imaging resolution. By effectively merging the phases reconstructed by TIE and WOTF in the frequency domain, the high-accuracy low-frequency phase “global” profile can be secured, and high-resolution high-frequency features can be well preserved simultaneously. Simulations and experimental results on a microlens array and unstained biological cells demonstrate the effectiveness of MTF. © 2021 Optical Society of America

<https://doi.org/10.1364/OL.422095>

In the field of biomedical microscopy, many samples of interest (e.g., unstained cells) are phase objects, showing little intensity contrast in conventional brightfield microscopy [1]. Although they can be made visible by specific staining or fluorescent labeling, the associated photobleaching and phototoxicity of the exogenous contrast agents prevent their continuous, long-term observation. Recently, quantitative phase imaging (QPI) has

received increased interest in optical microscopy research due to its capabilities to quantify optical thickness and morphologies of unlabelled samples [2].

The transport of intensity equation (TIE) is a well-established deterministic phase retrieval approach that can recover the quantitative phase by taking intensities of the sample at multiple axially defocused planes [3,4]. Recently, TIE has been increasingly adopted as a promising QPI tool due to its unique advantages over interferometric and iterative phase retrieval techniques: non-interferometric, non-iterative, phase-unwrapping-free, and compatible with the built-in Köhler illumination of a brightfield microscope [5,6]. Though there is no well-defined phase for partially coherent fields, the retrieved “phase” from TIE can be regarded as a generalized version, which is a scalar potential linking the phase gradient to the conditional frequency moment of the Wigner distribution function (WDF) [7,8]. When the illumination field satisfies the zero-moment condition, the generalized phase retrieved by TIE reduces to the well-defined phase as in the coherent case, reflecting the optical path length induced by the sample [4,8,9].

When a sample is illuminated with partially coherent light, TIE is expected to achieve improved spatial resolution beyond the coherent diffraction limit, as the angular spread of illumination contributes to the lateral resolution [10]. But the validity of TIE is posed under the paraxial approximation, limiting its applications to low-numerical-aperture (NA) imaging and slowly varying objects. Though a larger illumination NA provides a higher theoretical diffraction limit resolution, it generally leads to significant loss of high-frequency, precluding its application to high-resolution QPI [5,6,11]. Alternatively, QPI can be achieved by phase deconvolution based on the coherent contrast transfer function (CTF) [4,12] or partially coherent weak object transfer function (WOTF) [5,6,13] with the same input. Since the phase transfer function (PTF) can be derived without paraxial approximation, these methods are suitable for high-NA imaging. Specifically, WOTF linearizes the image formation

process in the frequency domain by ignoring bilinear terms (the first-order Born approximation). So they are generally limited to weakly scattering samples in which the phase delay induced by the object should be small (typically less than $\pi/2$) [5,6,14]. Consequently, high-resolution high-accuracy QPI of nonweak phase objects with small-scale features and large phase excursions remains a great challenge.

In this Letter, we propose a mixed-transfer-function (MTF) approach to solve the dilemma between accuracy and resolution. Deterministic phase-retrieval-based defocus variations can be interpreted independently of the spatial domain (as in TIE) [3,4] and spatial frequency domain (as in WOTF) [5,6,13]. For phase retrieval under quasi-monochromatic partially coherent illuminations with central wavelength λ , the paraxial transport of the intensity can be described by the generalized TIE (GTIE) defined in phase space [8]:

$$\frac{\partial I(\mathbf{x})}{\partial z} = -\lambda \nabla_{\mathbf{x}} \cdot \int \mathbf{u} W(\mathbf{x}, \mathbf{u}) d\mathbf{u}, \quad (1)$$

where $W(\mathbf{x}, \mathbf{u})$ is the WDF of the partially coherent field. \mathbf{x} is the transverse coordinates (x, y), and \mathbf{u} is the coordinate (u, v) in the frequency domain corresponding to \mathbf{x} . $I(\mathbf{x})$ is the intensity, and $\nabla_{\mathbf{x}}$ is the gradient operator over \mathbf{x} . Based on GTIE, the generalized phase $\hat{\phi}(\mathbf{x})$ is [8]

$$\frac{\int \mathbf{u} W(\mathbf{x}, \mathbf{u}) d\mathbf{u}}{\int W(\mathbf{x}, \mathbf{u}) d\mathbf{u}} = \frac{1}{2\pi} \nabla_{\mathbf{x}} \hat{\phi}(\mathbf{x}), \quad (2)$$

suggesting that the phase recovered by TIE is a scalar potential whose gradient gives the conditional frequency moment of the WDF. For optical microscopy, only the optical field in the image plane is accessible. So the phase retrieved by TIE is the generalized phase of the “image” [first-order conditional frequency moment of the WDF in the image plane, $W_{\text{image}}(\mathbf{x}, \mathbf{u})$], instead of the phase of the object, $\phi(\mathbf{x})$. Considering a slowly varying object imaged by a microscope with a finite aperture, $W_{\text{image}}(\mathbf{x}, \mathbf{u})$ can be expressed as [8,15]

$$W_{\text{image}}(\mathbf{x}, \mathbf{u}) \approx I(\mathbf{x}) \left| S \left[\mathbf{u} - \frac{1}{2\pi} \nabla_{\mathbf{x}} \phi(\mathbf{x}) \right] \right|^2 |P(\mathbf{u})|^2, \quad (3)$$

where $S(\mathbf{u})$ is the intensity of the incoherent effective source (condenser aperture), and $P(\mathbf{u})$ is the objective pupil function. From the geometric-optics perspective, Eq. (3) depicts a physical picture behind TIE in the spatial domain [Fig. 1(a1)]. The phase of a slowly varying sample can be approximated as a piecewise linear function (combination of prisms). The sample-induced phase modulation exhibits angle-shift invariance. At each position, the direction of each incident light is deflected by the amount of the sample phase gradient, and the angular spread of incident illumination is unaltered. But after collecting by an objective, only rays within the pupil can pass through the imaging system and contribute to image formation, leading to degradation in phase gradient estimation (the centroid of the shifted source inside the pupil is inconsistent with the true phase gradient) [Fig. 1(a2)] [4,8,16].

The derivation of the phase gradient can be quantified by the phase gradient transfer function (PGTF) [15,16], defined as the ratio between the measured phase gradient in the image plane and the ideal one of the object [4]. PGTFs

for a brightfield microscope with different coherence parameters $s = \text{NA}_{\text{ill}}/\text{NA}_{\text{obj}}$ (NA_{ill} and NA_{obj} are illumination and objective NAs) are plotted in Fig. 1(a3) (the spatial frequency coordinate is normalized against $\text{NA}_{\text{obj}}/\lambda$), revealing the underestimation of the phase gradient appearing when its value is larger than $1-s$, while small-gradient components remain intact [4,8,16]. It suggests two vital features of TIE under partially coherent fields: first, partial coherence results in high-frequency attenuation as s is increased, leading to blurry phase retrievals. Second, a sufficiently smooth phase can be accurately recovered by TIE, regardless of the total phase delays.

Alternatively, deterministic phase retrieval can be realized by phase deconvolution based on WOTF under partially coherent illuminations [5,6,13]. The use of a “weak object” in WOTF suggests its reliance on the first-order Born approximation. When satisfied, the Fourier spectrum of the intensity captured at a defocused distance z can be represented as [6]

$$\tilde{I}_z(\mathbf{u}) = I_0 [\delta(\mathbf{u}) + \text{ATF}_z(\mathbf{u}) \tilde{\eta}(\mathbf{u}) + \text{PTF}_z(\mathbf{u}) \tilde{\phi}(\mathbf{u})], \quad (4)$$

here $I_0 \delta(\mathbf{u})$ is the contribution from the average intensity in the in-focus plane, $\tilde{\eta}(\mathbf{u})$ and $\tilde{\phi}(\mathbf{u})$ are the Fourier transforms of the absorption and phase, respectively, and $\text{ATF}_z(\mathbf{u})$ and $\text{PTF}_z(\mathbf{u})$ are amplitude and phase transfer functions (real and imaginary parts of the WOTF, respectively) [6]:

$$\begin{aligned} \text{WOTF}_z(\mathbf{u}) &= \iint S(\mathbf{u}') |P(\mathbf{u}' + \mathbf{u})| |P(\mathbf{u}')| \\ &\times e^{ikz(\sqrt{1-\lambda^2(\mathbf{u}'+\mathbf{u})^2} - \sqrt{1-\lambda^2\mathbf{u}'^2})} d\mathbf{u}', \end{aligned} \quad (5)$$

$$\text{ATF}_z(\mathbf{u}) = \text{Re}[\text{WOTF}_z(\mathbf{u})], \quad (6)$$

$$\text{PTF}_z(\mathbf{u}) = -\text{Im}[\text{WOTF}_z(\mathbf{u})]. \quad (7)$$

Subtracting two defocused intensities $\pm z$ can cancel the contribution of absorption and obtain the invertible relationship between the phase and intensity difference. Figure 1(b1) shows that phase deconvolution methods provide an alternative interpretation of deterministic phase retrieval in the spatial frequency domain. The phase of a weak scattering sample can be decomposed as sinusoidal gratings with different frequencies. The

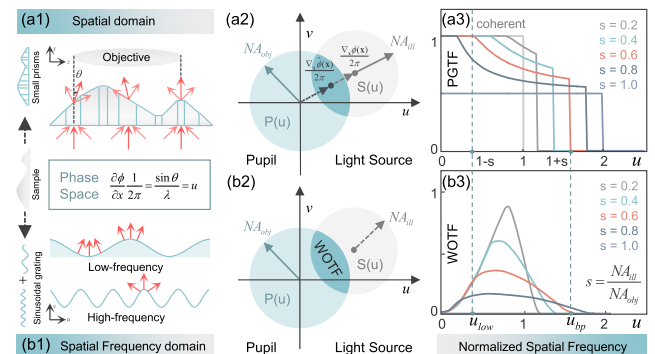


Fig. 1. (a1), (b1) Physical implications of TIE and WOTF. (a2), (b2) Geometric illustrations for deriving the PGTF [4] and WOTF [13,15,16], given by the overlap of the objective pupil and the displaced effective source. (a3), (b3) PGTF and WOTF for phase imaging under different coherence parameters s .

attenuation effect of the imaging system with different frequencies is quantified by WOTF, which is calculated as the overlap of a shifted effective source and pupil function [Fig. 1(b2)]. The key advantage of such methods is enabling high-NA imaging, as they can be derived in nonparaxial conditions. Also, phase deconvolution directly compensates for attenuation at higher spatial frequencies, resulting in high-resolution QPI. But these methods based on the direct inversion of WOTF suffer from low-frequency inaccuracies due to the low amplitude of the PTF at low frequency [Fig. 1(b3)], and more importantly, the violation of the weak object assumption when imaging a thick sample. It should be mentioned that the linearized relation between intensity and phase [Eq. (4)] can also be derived by the first-order Rytov approximation [5,14,17], which requires the phase to be slowly varying, imposing a less stringent requirement on the phase magnitude and extending the validity of WOTF to objects with relatively large phases [5,18]. But for thick objects (phase delay significantly exceeding $\pi/2$), both the Born and Rytov approximations tend to provide poor phase retrieval accuracy [5,17].

Despite the formal similarity between PGTF and WOTF, the TIE and phase deconvolution methods provide two distinct perspectives of deterministic phase retrieval from the spatial domain and spatial frequency domain, respectively. As indicated by Eqs. (1)–(3), the phase-space representation of GTIE and generalized phase connects the phase gradient to the spatial frequency shift. The correspondence implies the equivalence of deflection (prisms) and diffraction (gratings)—they both change the directions of incident rays. For the two different transfer functions, it is recognized that the two methods are complementary concerning the range of applicability. TIE is established under the paraxial approximation and valid for thick, slowly varying samples, while WOTF assumes a weakly scattering object and is valid under nonparaxial conditions. This inspires us to properly combine these two approaches to ensure complementarity, mutual reinforcement, and respective advantages.

A simulated example is provided to explain the basic principle of MTF. The simulated phase is a “TIE” logo superimposed on a smooth Gaussian function with a large phase range (0–5 rad) [Fig. 2(a1)]. The absorption is also a smooth Gaussian function, resulting in nonuniform intensity (0.7–1) [Fig. 2(a2)]. The image formation under partially coherent illumination ($\lambda = 550$ nm, $NA_{\text{obj}} = 0.45$, $s = 0.7$) was simulated based on Abbe’s method. Two defocused intensities (± 1.5 μm) are created by applying the angular spectrum method. The in-focus intensity and difference between two defocused intensity images serve as the input of TIE and WOTF [step 1 in Figs. 2(b1) and 2(b2)], producing two phase retrievals independently [step 2 in Figs. 2(c1) and 2(d1)]. The reconstruction errors of these two methods are shown in Figs. 2(c2) and 2(d2) and Figs. 2(c3) and 2(d3). The metric used to measure the accuracy of phase retrieval is the root mean square error (RMSE) (quantifies the overall difference between the true phase and retrieved one) and the structural similarity index measure (SSIM) (quantifies the phase quality degradation caused by losses in high-frequency features).

As predicted by our previous analysis, TIE can recover the smooth component accurately (low RMSE of 0.0614) but failed to retrieve details (relatively small SSIM of 0.9976) [Fig. 2(c)]. In contrast, the WOTF retrieved phase preserves

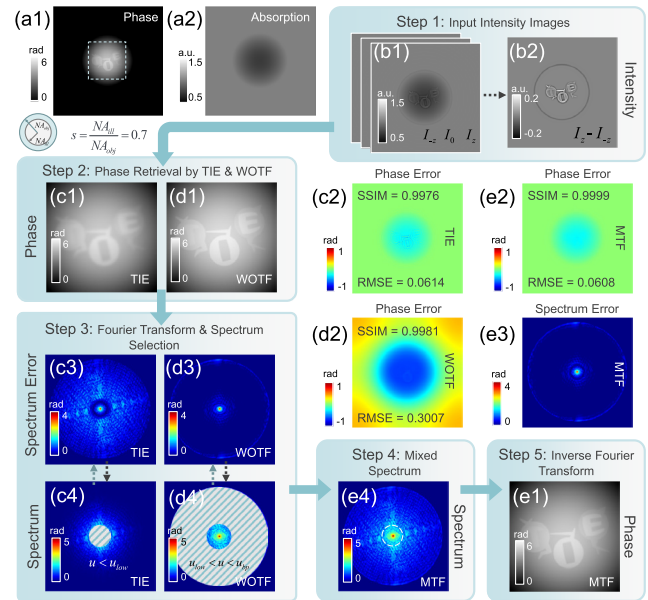


Fig. 2. (a1), (a2) True phase and absorption. (b1), (b2) Input intensities. (c1)–(e1) Phases retrieved by TIE, WOTF, and MTF. (c2)–(e2) Phase errors of the results obtained by TIE, WOTF, and MTF. (c3)–(e3) Phase spectrum errors of the results recovered by TIE, WOTF, and MTF. (c4)–(e4) Fourier spectrum of the phases retrieved by TIE, WOTF, and MTF.

fine features well (SSIM of 0.9981), but suffers from inaccurate low-frequency (large RMSE of 0.3007) [Fig. 2(d)]. For thick objects with fine details, these methods have complementary advantages at low (in TIE) or high (in WOTF) frequencies. Thus, we merged the low frequencies of the TIE retrieved phase with the high-frequency counterparts of WOTF in the frequency domain based on complementary filters [steps 3 and 4 in Fig. 2]. Figures 1(a3) and 1(b3) show that the cutoff frequency u_{low} can be naturally set to $(1 - s)NA_{\text{obj}}/\lambda$, corresponding to the limit of the undistorted gradient in PGTF. Finally, the phase recovered by inverse Fourier transform of the mixed spectrum [step 5 in Fig. 2(e1)] has a high-precision, low-frequency profile with well-preserved high-frequency features (RMSE of 0.0608, SSIM of 0.9999), proving that MTF can overcome the contradiction between accuracy and resolution.

Experiments were implemented based on a brightfield microscope (IX83, Olympus) equipped with an industrial camera (DMK33UX226, 1.85 μm pixel pitch). The illumination from a widely open condenser (s is set to 0.7 in all experiments) is filtered by a green interference filter (central wavelength $\lambda = 550$ nm) to create quasi-monochromatic spatially partially coherent illumination. In the first experiment, a microlens array (Nr. 18-00036, pitch = 30 μm , ROC = 9.67 mm \pm 5%) was measured with a $10\times$, 0.25 NA objective. Figures 3(a1)–3(c1) present the results recovered by WOTF, TIE, and MTF using the in-focus image and two defocus images at ± 1.95 μm . The regions of interest with fine details (highlighted by arrows) are shown in Figs. 3(a3)–3(c3). Figures 3(a4)–3(c4) show profiles across the center of a single lens [Figs. 3(a1)–3(c1)]. Figures 3(a2)–3(c4) illustrate the fine details can be clearly resolved by WOTF, but the lens height was underestimated. The lens profile recovered by TIE is in good accordance with the manufacturer’s specifications, while details were smooth out. In

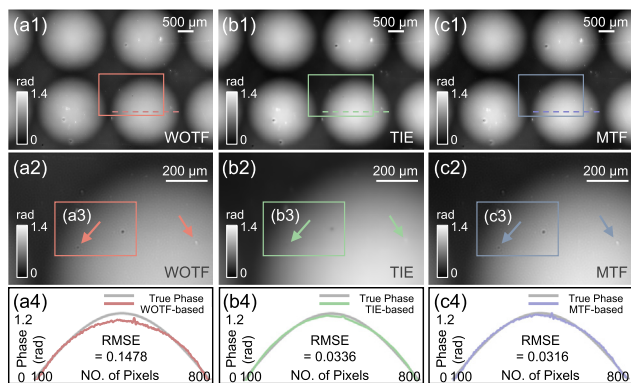


Fig. 3. (a1)–(c1) Recovered phase of the microlens array by using WOTF, TIE, and MTF. (a2)–(c2) Enlarged view corresponding to boxes in (a1)–(c1). (a3)–(c3) Regions of interest with fine details. (a4)–(c4) Profiles corresponding to dashed lines in (a1)–(c1).

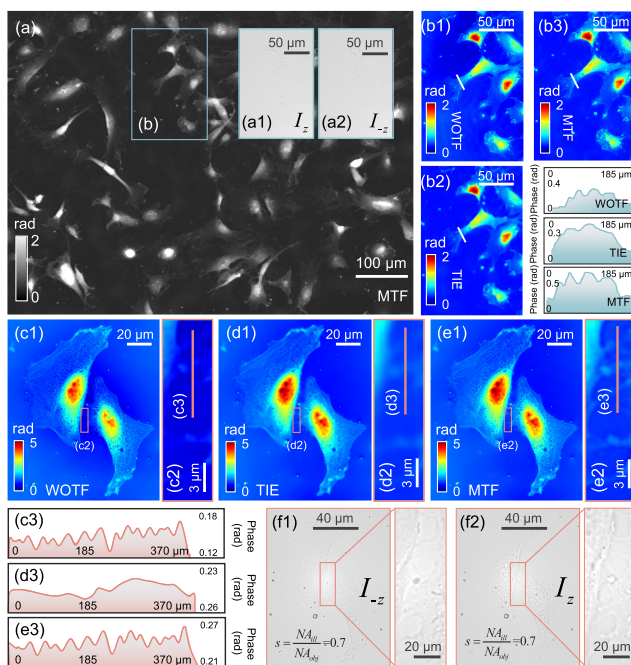


Fig. 4. (a) Phase of 3T3-L1 cells retrieved by MTF with a $10\times$, 0.25 NA objective. (a1), (a2) Defocused intensities corresponding to (b). (b1)–(b3) Phase results corresponding to (b) by using WOTF, TIE, and MTF. (c1)–(e1) Recovery phase of HeLa cells with a $40\times$, 0.65 NA objective by WOTF, TIE, and MTF. (c2)–(e2) Enlarged views corresponding to boxes in (c1)–(e1). (c3)–(e3) Profiles corresponding to lines in (c2)–(e2). (f1), (f2) Defocused intensities of HeLa cells.

contrast, MTF correctly recovered the lens profile, and the fine details were well preserved.

Finally, we demonstrate the potential of MTF for high-resolution QPI of unstained biological samples. Unstained 3T3-L1 cells can be clearly visualized by MTF using two images with slight defocusing ($\pm 1.5 \mu\text{m}$), resulting in a high-contrast QPI revealing sub-cellular structures [Fig. 4(a)]. A comparison of phase retrieval results obtained by WOTF, TIE, and MTF is presented in Figs. 4(b1)–4(b3), which almost reproduced the simulation results. WOTF produced a sharp image with low-frequency component underestimation. In contrast, TIE

retrieved plump cell profiles with blurred boundaries and details. When MTF was applied, the details lost in the TIE reconstruction results were restored, resulting in a high-quality phase retrieval with both high accuracy and sharp details. Similar conclusions can be drawn from the phase retrievals of unstained HeLa cells under a higher magnification objective ($40\times$, 0.65 NA) [Figs. 4(c1)–4(e3)]. Note that the phase range of HeLa cells typically exceeds 5 rad (cannot be considered as weak phase objects), suggesting that the validity of MTF can extend far beyond the weak phase regime.

In conclusion, we have proposed the MTF approach to overcome the contradiction between measurement accuracy and imaging resolution in TIE and WOTF phase retrieval. By properly merging the phases reconstructed by these two approaches in the frequency domain, MTF is capable of achieving high-resolution high-accuracy QPI for nonweak phase objects with fine details and large phase excursions. The effectiveness of MTF has been demonstrated by measuring a microlens array and unstained biological cells. In the future, we will extend MTF to single-shot speckle-based QPI [9] and further enhance its imaging resolution by using annular illuminations [6].

Funding. National Natural Science Foundation of China (61905115); Leading Technology of Jiangsu Basic Research Plan (BK20192003); National Defense Science and Technology Foundation of China (2019-JCJQ-JJ-381); Youth Foundation of Jiangsu Province (BK20190445); Fundamental Research Funds for the Central Universities (30917011204, 30920032101).

Disclosures. The authors declare no conflicts of interest.

Data Availability. Data underlying the results presented in this paper are not publicly available at this time but may be obtained from the authors upon reasonable request.

REFERENCES

- Y. Park, C. Depeursinge, and G. Popescu, *Nat. Photonics* **12**, 578 (2018).
- A. Barty, K. Nugent, D. Paganin, and A. Roberts, *Opt. Lett.* **23**, 817 (1998).
- M. R. Teague, *J. Opt. Soc. Am.* **73**, 1434 (1983).
- C. Zuo, J. Li, J. Sun, Y. Fan, J. Zhang, L. Lu, R. Zhang, B. Wang, L. Huang, and Q. Chen, *Opt. Laser Eng.* **135**, 106187 (2020).
- M. H. Jenkins and T. K. Gaylord, *Appl. Opt.* **54**, 8566 (2015).
- C. Zuo, J. Sun, J. Li, J. Zhang, A. Asundi, and Q. Chen, *Sci. Rep.* **7**, 7654 (2017).
- D. Paganin and K. A. Nugent, *Phys. Rev. Lett.* **80**, 2586 (1998).
- C. Zuo, Q. Chen, L. Tian, L. Waller, and A. Asundi, *Opt. Laser Eng.* **71**, 20 (2015).
- L. Lu, J. Sun, J. Zhang, Y. Fan, Q. Chen, and C. Zuo, *Front. Phys.* **7**, 77 (2019).
- E. Barone-Nugent, A. Barty, and K. Nugent, *J. Microsc.* **206**, 194 (2002).
- T. Chakraborty and J. C. Petrucci, *Opt. Express* **25**, 9122 (2017).
- P. Cloetens, W. Ludwig, J. Baruchel, D. Van Dyck, J. Van Landuyt, J. Guigay, and M. Schlenker, *Appl. Phys. Lett.* **75**, 2912 (1999).
- C. J. Sheppard, *J. Opt. Soc. Am. A* **21**, 828 (2004).
- Y. Sung, W. Choi, C. Fang-Yen, K. Badizadegan, R. R. Dasari, and M. S. Feld, *Opt. Express* **17**, 266 (2009).
- S. B. Mehta and C. J. Sheppard, *J. Opt. Soc. Am. A* **35**, 1272 (2018).
- C. J. Sheppard, *J. Opt. Soc. Am. A* **35**, 1846 (2018).
- T. E. Gureyev, T. J. Davis, A. Pogany, S. C. Mayo, and S. W. Wilkins, *Appl. Opt.* **43**, 2418 (2004).
- S. S. Kou, L. Waller, G. Barbastathis, P. Marquet, C. Depeursinge, and C. J. Sheppard, *Opt. Lett.* **36**, 2671 (2011).